

Plotting time: On the usage of CNNs for time series classification

Nuno M. Rodrigues¹, João E. Batista¹, Leonardo Trujillo² and Bernardo Duarte^{3,4}
and Mario Giacobini⁵ and Leonardo Vanneschi⁶ and Sara Silva¹

¹LASIGE, Faculdade de Ciências da Universidade de Lisboa, Campo Grande, 1749-016 Lisboa, Portugal

²Departamento de Ingeniería Eléctrica y Electrónica, Tecnológico Nacional, México/IT de Tijuana

³MARE - Marine and Environmental Sciences Centre, Faculdade de Ciências da Universidade de Lisboa, Campo Grande, 1749-016 Lisboa, Portugal

⁴Departamento de Biologia Vegetal, Faculdade de Ciências da Universidade de Lisboa, Campo Grande, 1749-016 Lisboa, Portugal

⁵Data Analysis and Modeling Unit, Department of Veterinary Sciences, University of Torino, Italy

⁶NOVA Information Management School (NOVA IMS), Universidade Nova de Lisboa, Campus de Campolide, 1070-312 Lisboa, Portugal

{nmrodrigues, jebatista, baduarte, sara}@fc.ul.pt, leonardo.trujillo@tectijuana.edu.mx,
mario.giacobini@unito.it, lvanneschi@novaims.unl.pt

Abstract

We present a novel approach for time series classification where we represent time series data as plot images and feed them to a simple CNN, outperforming several state-of-the-art methods.

We propose a simple and highly replicable way of plotting the time series, and feed these images as input to a non-optimized shallow CNN, without any normalization or residual connections. These representations are no more than default line plots using the time series data, where the only pre-processing applied is to reduce the number of white pixels in the image. We compare our method with different state-of-the-art methods specialized in time series classification on two real-world non public datasets, as well as 98 datasets of the UCR dataset collection. The results show that our approach is very promising, achieving the best results on both real-world datasets and matching / beating the best state-of-the-art methods in six UCR datasets. We argue that, if a simple naive design like ours can obtain such good results, it is worth further exploring the capabilities of using image representation of time series data, along with more powerful CNNs, for classification and other related tasks.

1 Introduction

Time series classification (TSC) problems are highly diverse in nature, covering a wide range of domains. Recently, this field of study is receiving more and more attention, arguably due to the creation of large data repositories such as UCR [Dau *et al.*, 2018]. Such easy availability of data motivated the proposal of multiple new algorithms to address TSC.

When looking at the current state-of-the-art (SOTA) of TSC, led by the HIVE-COTE or TS-CHIEF methods, or even just the more popular algorithms for TSC, there are two main approaches. Some algorithms like BOSS, BOP or WEASEL use word and symbol embeddings along with sliding windows to transform the data [Schäfer, 2014; Large *et al.*, 2018; Schäfer and Leser, 2017]. The other predominant approach is to use different ensemble methods, such as HIVE-COTE (which includes BOSS), TS-CHIEF or Proximity Forests [Lines *et al.*, 2016; Lucas *et al.*, 2019; Shifaz *et al.*, 2020].

Recently, a new trend is emerging due to the rising popularity of convolutional neural networks (CNN), which is the use of convolution operations. We can see this in ROCKET [Dempster *et al.*, 2020], which applies random convolutional kernels to the time series data, or in InceptionTime, which is an actual computer vision model [Karimi-Bidhendi *et al.*, 2018; Fawaz *et al.*, 2020].

The vast majority of these algorithms share one common trait: they use the numeric data of the time series to find pat-

terns and induce models. However, pattern recognition can also be tackled from a computer vision perspective, using visual representations of the data. As previously mentioned, and further elaborated, there are already some recent algorithms that use a visual representation of the data to perform TSC. However, we argue that these works follow an overly complex path, and we propose a much simpler approach.

Our work demonstrates that, with highly simplistic visual representations of the time series data, it is possible to achieve results that are equal or even better than the ones obtained by the best SOTA methods available today.

2 Related work

There are two general goals when non-image data is converted to a 2D image representation. The first one is to understand and interpret the data, since converting it to a visual representation allows a researcher to analyze the data in a more human-readable form. These techniques have a long history in pattern analysis and machine learning [Keim, 2000], including different types of geometric representations, pixel-oriented visualizations and dimensionality reduction techniques. For instance, a popular SOTA method is t-SNE [van der Maaten and Hinton, 2008], that allows for 2D and 3D representations of large datasets in high-dimensional spaces. While t-SNE focuses on visualizing an entire dataset, General Line Coordinates (GLC), on the other hand, can be used to represent individual data samples as polylines [Kovalerchuk, 2018], without any loss of information.

The second broad reason for transforming non-image data into images is that it allows researchers to solve the original learning problem using powerful and widely available computer vision algorithms, such as CNNs. This approach is much more recent, with a growing but still fairly small literature on the subject. In [Dovhalets *et al.*, 2018] the authors used GLC representations of data to pose an image recognition problem and solved it with CNNs, achieving similar performance compared to solving the original problem directly, with the added benefit that interpreting the results is easier. RNA data is transformed into 2D images in [Lyu and Haque, 2018], outperforming previous works on the same problem, while using a domain specific transformation of the data. A notable approach is DeepInsight [Sharma *et al.*, 2019], that proposes a general methodology to transform data samples into unique images and subsequently applies CNN to a variety of problems from different domains. DeepInsight transforms the data by applying Principal Component Analysis in a simple but creative manner, and also produces informative visualizations of

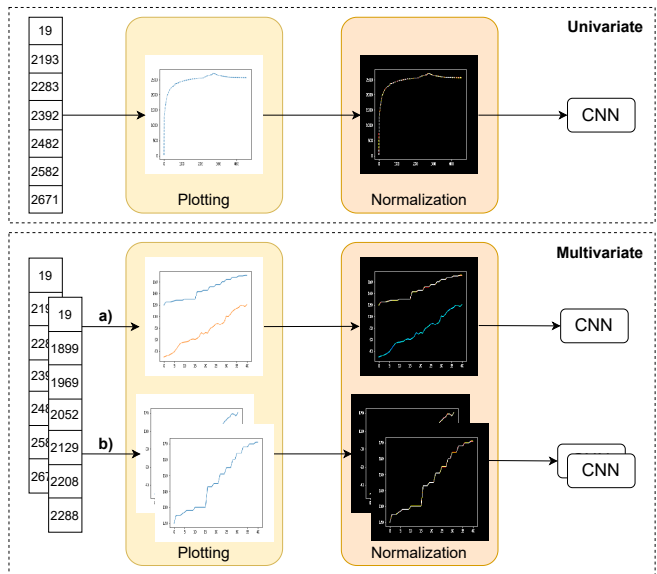


Figure 1: The proposed methodology. For univariate time series, each series is converted into an image, normalized and given to a CNN. For multivariate time series, we test two approaches: **a)** all series are displayed on the same plot and given to a single CNN; **b)** different series are displayed in separate plots and given to siamese CNNs, whose output is concatenated before flattening. We also split the multivariate cases in multiple univariate problems, for comparison.

the samples in a dataset, intended to provide unique *insights* on the problem. Regarding the case of time series classification, [Karimi-Bidhendi *et al.*, 2018] transforms the time series to a Gramian Angular Difference Field (GADF), a visual representation of the data that is subsequently processed by Google’s pre-trained Inception CNN, achieving SOTA results.

3 Proposed methodology

The methodology we propose is more focused on the transformation of the time series data into image data, and less on the particulars of the CNN architecture. Figure 1 illustrates the different steps of the methodology, in both univariate and multivariate cases. Details of each step are provided below.

3.1 Generating image data from time series

We follow a simple and replicable process of transforming the time series data into image plots to be used by the CNN. First, the time series data is loaded without any pre-processing. Then, using *matplotlib* library [Hunter, 2007] we plot each time series adopting the default parameters, obtaining a 432×288 sized image for each series, as seen in Figure 1. The plot axes are included in the image, along with their problem specific time (x -axis) and value (y -axis) numbers, since they can provide important information, as shown later when we analyse feature maps. Notice that not all the time series are

required to have the same length, since this has no impact when transforming the data into an image, and does not imply loss of valuable information (this way avoiding the need to oversample the data).

3.2 Normalizing the image data

When loading the plots to use as input to our networks, we perform two kinds of image pre-processing. We start by the standard rescaling of pixel values to the $[0, 1]$ range, and then we apply a samplewise standard normalization. The samplewise normalization essentially inverts the colors (produces a negative of the original image, as shown in Figure 1), which reduces the amount of empty white space by turning the pixel values to 0 (black). This reduces the activations of the feature maps in empty areas where there is no information, while increasing them in the numbers of the axes, which is helpful as they also contain information. This normalization produces large improvements in both learning and generalization. Its effect on the feature maps will be analysed in Section 5.

3.3 Feeding the plots to the CNN

For all the problems addressed, we use a simple shallow CNN of five convolutional and pooling layers, interspersed, and three fully connected layers with two dropouts in between. As for the hyperparameters, we use standard values and do not perform any sort of grid-search / bayesian hyperparameter optimization. Regarding the filters, we start with 16 and double the number in each convolutional layer. In the first and second fully connected layers we use 256 and 128 units, respectively. For the optimizer we use ADAM with a learning rate of 0.001.

When modeling a problem, if its data is univariate (containing only one time series) we simply feed the pre-processed images to a CNN like the one described above (top part of Figure 1). For multivariate problems (data containing more than one time series) we test different approaches, identified as a) and b) in the bottom half of Figure 1. In variant a) the different time series for the same sample are displayed on the same plot and given to a single CNN as the one used for the univariate approach. In variant b) the different time series are displayed in separate plots and given to a set of siamese CNNs. Each input head has the same set of convolutional and pooling layers described above and, before flattening, the outputs of these networks are concatenated and fed into the same classifier section, producing a single output. This method allows for different features to be extracted from the different time series, however, it is far more computationally expensive.

There is also an additional variant, not shown in the figure, which is to split the multivariate problems in multiple

univariate problems, each one using only one time series. We have included this last variant because we wanted to check that drawing more than one time series in a single plot, or using a set of siamese networks, is not a confounding factor that prevents the learning of the information contained in each variable. Since our multivariate datasets have only two time series, it was feasible to do so.

4 Experiments

All experiments were performed on a Windows 10 machine with one NVIDIA 2080 TI GPU with 11GB of RAM. All network based models were implemented in TensorFlow.

4.1 Datasets and Problems

Here we describe the datasets used to test our methodology. Since the UCR dataset is public domain and is already described in its website, we provide more details on the remaining two datasets and respective prediction tasks.

OPTOX

The OPTOX dataset was collected by the Marine and Environmental Sciences Centre - MARE - Faculty of Sciences, University of Lisbon. Each sample corresponds to a chlorophyll fluorescence induction curve, and contains the fluorescence values taken at different time steps from a model diatom used in ecotoxicology (*Phaeodactylum tricorutum*) exposed to 13 different emerging contaminants at different concentrations, following the international standards for ecotoxicological assays. For each concentration, 30 independent replicates were obtained. Details of the experiments and samples can be found in [Silva *et al.*, 2020].

With this dataset, we address the challenge of identifying which of the 13 contaminants is detected, using only the fluorescence induction curve. Table 1 contains more detailed information regarding this dataset, including the identification of the contaminants, number of concentrations considered for each, and number of samples per class.

FISIO

The FISIO dataset was collected by the Centre of Preventive Medicine and Sport - SUIISM - University Structure of Hygiene and Sport Sciences, Centre of excellence of the University of Turin. Data were recorded during an indoor trial conducted by the centre, where a group of 262 volunteers underwent an aerobic exercise on a trade mill. The test started with a speed of 5 km/h that was incremented by 1 km/h every minute. The participant could suspend the test when he/she

Table 1: OPTOX dataset summary, containing the class names (contaminants) concentrations considered for each contaminant, and distribution of the total number of samples per class.

Contaminant	#concentrations	#samples
Diclofenac	6	180
Fluoxetine	6	180
Glyphosate	6	180
Ibuprofen	6	180
Propranolol	6	180
Sodium Dodecyl Sulphate (SDS)	5	150
Triclosan	6	180
Dissolved Ionic Copper	4	120
Copper Engineered Nanoparticles	4	120
Dissolved Ionic Zinc	4	120
Zinc Engineered Nanoparticles	4	120
Dissolved Ionic Titanium	4	120
Titanium Engineered Nanoparticles	4	120

Table 2: FISIO dataset summary, containing the distributions of samples per class for the two problems addressed, BMI and Age.

BMI		Age	
Class 1	Class 2	Class 1	Class 2
221	41	128	134

felt exhausted. Cardio-respiratory variables were recorded every 10 seconds, namely heart rate (HR) and ventilation (VEN), along with the age, gender and body mass index (BMI) of each participant. More details on this dataset and related tests can be found in [Azzali *et al.*, 2020].

With this dataset, we addressed two challenges: based on both HR and VEN, we predict 1) BMI class: two classes were defined, based on the UK NHS BMI charts for both children and adults (since some of the participants were underage), where Class 1 contains Underweight and Healthy participants, and Class 2 contains Overweight and Obese participants; 2) Age class: two classes were defined, with Class 1 for participants younger than 30 years old and Class 2 for all the others. Gender remained unused.

Table 2 contains the information regarding sample distribution per class for both problems. Since we had both time series (HR and VEN) for each participant, we decided to use both multivariate and univariate approaches (Section 3.3).

UCR

The UCR archive contains, as of now, a set of 128 univariate and 30 multivariate datasets [Dau *et al.*, 2018]. From the 128 univariate problems we tested our approach on 98 of them. The selection criterion for these 98 problems was two-fold. First, because the results provided by UCR for each classifier do not include all 128 problems, we decided to use only the problems that were tested with all the algorithms, ending up with 108 problems. Second, due to time constraints, we decided to not test our approach on single axis data of multi-axes problems (*e.g* Cricket X/Y/Z), ending with the final

amount of 98 problems. Regarding the multivariate problems, the archive does not have results to compare to, so we did not use them.

4.2 Methods

In order to have comparison grounds for our methodology, we tested a set of different classifiers for both the OPTOX and the FISIO datasets: XGBoost [Chen and Guestrin, 2016], Random Forests (RF) [Breiman, 2001], deep learning classifiers 1D CNN and a deep ANN, and ROCKET.

The FISIO dataset presented an additional problem for these classifiers, as it consists of a multivariate problem with time series of different lengths. To address this issue, we truncated each time series to the same length as the smallest one of that type, therefore assuming the risk of losing information. This problem serves to highlight the advantage of our methodology in being able to use the full time series without the need for all the series to have the same length.

We performed 30 independent runs with all the methods, with an 80/20 split for training and test, each with a seed equal to the number of the run. For each run, both XGBoost and RF were optimized by means of grid-search for the following parameters: max depth; number of estimators; tree method; learning rate; criterion.

As for UCR, the archive already provides results based on 30 independent runs from several other algorithms. Due to the limited computational resources and large amount of problems, we started by performing five independent runs per problem, and an additional 25 only in those problems where our methodology was able to outperform or tie as the best result.

5 Results and Discussion

Here we compare the results obtained by our approach with the results of several other methods, including the current SOTA, on the OPTOX, FISIO and UCR datasets. Statistically significant differences in the results are determined by the Kruskal-Wallis test at $p < 0.01$. We use a non-parametric test because not all the results follow a normal distribution. When the results presented in tables identify more than one value as the best, it means the difference between them is not statistically significant. All the p -values are included in the Appendix, in Table 7 for OPTOX, Tables 8 to 15 for FISIO, and Tables 16 to 21 for the UCR problems where we performed 30 runs (see Section 4.2). This section also discusses the effect that image data normalization has on the learned features by examining feature maps extracted from the CNNs.

Table 3: Median overall accuracy of all methods on the OPTOX problem. The best test result is represented in **green**.

	RF	XGBoost	ROCKET	ANN	1D CNN	CNN Log	CNN
Train	0.9625	0.9983	0.9991	0.8493	0.9993	0.9807	0.9815
Test	0.7461	0.8076	0.9705	0.9089	0.9641	0.9765	0.9732

OPTOX

For this dataset, we have produced two sets of results from our methodology, identified as CNN and CNN Log. In CNN, the values of the different time steps are drawn at equally spaced intervals on the x -axis of the plots, even if in reality the time intervals between every two measurements are not the same for the entire curve. By convention, when visualizing an induction curve it is common to use a logarithmic scale on the x -axis, which is what CNN Log does.

Table 3 compares all tested classifiers in terms of median accuracy in both training and test sets for the contaminant prediction task of the OPTOX dataset. As shown, our algorithm outperformed all the other methods. CNN Log was the best performing method, significantly better than CNN, which is tied in second with ROCKET. This difference between CNN and CNN Log highlights the need to take into consideration domain knowledge when transforming the data into images. Despite not changing the methodology whatsoever, this change in scale significantly improved the results.

FISIO

Table 4 compares all tested classifiers in terms of median accuracy in both training and test sets, for the BMI and Age problems of the FISIO dataset. The results identified as HR and VEN are the ones obtained using only one of the time series (the additional variant mentioned in Section 3.3). The results identified as HR+VEN refer to variant a), where both time series are drawn in the same plot, and the ones identified as Siamese refer to variant b), where each time series is drawn in a different plot and the two plots are given to siamese networks.

On the BMI classification problem, the CNNs using only the HR time series obtained the best median result, but not significantly different from the results of RF and XGBoost. This provides two interesting findings: for a multivariate problem, the best results were obtained using only one of the time series, supporting the hypothesis that using multiple time series may indeed be a confounding factor (for 1D CNN, HR+VEN certainly is); two standard classification methods were able to outperform not only all other deep learning classifiers, but also ROCKET, which is one of the top algorithms for TSC.

Regarding the Age classification problem, the best median

Table 4: Median overall accuracy from all models in the BMI and Age problems of the FISIO dataset. The best test result for each problem is represented in **green**.

	BMI							
	HR		VEN		HR+VEN		Siamese	
	Train	Test	Train	Test	Train	Test	Train	Test
RF	0.8564	0.8301	0.9090	0.8113	0.9138	0.8113	---	---
XGBoost	0.8562	0.8301	0.9371	0.8301	0.9251	0.8301	---	---
ROCKET	1	0.7264	1	0.7547	1	0.7169	---	---
ANN	0.9330	0.7641	0.9617	0.7924	0.9760	0.7735	0.8492	0.8113
1D CNN	1	0.6792	1	0.6981	0.5100	0.46	1	0.7547
CNN	1	0.8461	1	0.8269	1	0.8269	1	0.8365

	Age							
	HR		VEN		HR+VEN		Siamese	
	Train	Test	Train	Test	Train	Test	Train	Test
RF	0.9569	0.6037	0.9377	0.6037	0.9808	0.6415	---	---
XGBoost	0.9730	0.6037	0.9491	0.6320	1	0.6792	---	---
ROCKET	1	0.6132	1	0.5849	1	0.6981	---	---
ANN	0.8947	0.6415	0.9282	0.6037	0.9665	0.6981	0.7775	0.6981
1D CNN	1	0.5660	1	0.5849	1	0.6698	0.9952	0.6792
CNN	1	0.7058	1	0.6568	1	0.7058	1	0.7058

accuracy was obtained by the CNNs, who achieved the exact same value using only the HR time series, using both HR+VEN on the same plot, and following the siamese approach. When using only the HR time series, the CNNs outperformed all other methods, which did not happen with the other two approaches where, despite having a higher median accuracy, CNNs were not significantly different from the other highlighted classifiers.

UCR

Table 5 compares the number of times that each method, both the ones provided by UCR and ours, achieved first, second or third ranking on the set of 98 problems addressed. We can see that, although it is clearly not the best, our approach is able to challenge the current SOTA methods, beating / matching them on six problems, and arriving in third on another.

As mentioned in Section 4.2, in order to assess the results on such a large number of datasets, we performed five independent runs on all addressed problems, and then compared the best test accuracy achieved on each problem (between our five runs and UCR’s reported 30 runs per method). The six problems where CNN matched/beat the other methods on this comparison are BME, Coffee, Earthquakes, Plane, Smooth-Subspace and Trace (see Appendix, Table 22). For these six problems, we performed our additional 25 independent runs, and compared the median test accuracy of the 30 runs with the median results provided by UCR. As shown in Table 6, CNN achieved the best results in all these problems.

The effect of normalizing image data

Before deciding to apply the samplewise normalization described in Section 3.2, we performed some trial runs where the only pre-processing of image data was the rescaling of the pixel values. The main difference we observed was that, with-

Table 5: Number of times each method achieved first, second or third ranking spot in the UCR problems.

	CNN	TS-CHIEF	HIVE-COTE	ROCKET	InceptionTime	STC	ResNet	ProximityForest	WEASEL	S-BOSS	cBOSS	BOSS	RISE	TSF	Catch22
First	6	35	32	26	31	21	25	23	20	20	20	18	12	14	11
Second	0	6	9	10	12	2	9	4	7	4	2	4	1	2	1
Third	1	7	5	12	5	6	11	4	5	4	3	3	0	1	5

Table 6: Median overall test accuracy in the selected UCR problems. The best results for each problem are highlighted in green.

	CNN	TS-CHIEF	HIVE-COTE	ROCKET	InceptionTime	STC	ResNet	ProximityForest	WEASEL	S-BOSS	cBOSS	BOSS	RISE	TSF	Catch22
BME	<u>0.9133</u>	<u>0.9133</u>	0.9867	<u>0.9133</u>	<u>0.9133</u>	0.9400	<u>0.9133</u>	<u>0.9133</u>	0.9600	0.876	0.7733	0.8667	0.7933	0.9733	0.9133
Coffee	<u>0.7410</u>	<u>0.7410</u>	<u>0.7482</u>	<u>0.7482</u>	<u>0.7410</u>	0.7410	<u>0.7194</u>	<u>0.7518</u>	<u>0.7482</u>	<u>0.7482</u>	<u>0.7482</u>	<u>0.7482</u>	<u>0.7482</u>	<u>0.7482</u>	<u>0.7410</u>
Earthquakes	<u>0.7698</u>	0.7482	0.7482	0.7482	0.7410	0.7410	0.7194	0.7518	0.7482	0.7482	0.7482	0.7482	0.7482	0.7482	0.7410
Plane	<u>0.9905</u>	<u>0.9905</u>	<u>0.9905</u>	<u>0.9905</u>	<u>0.9905</u>	<u>0.9905</u>	<u>0.9905</u>	<u>0.9905</u>							
SmoothSubspace	<u>0.9867</u>	<u>0.9867</u>	0.9867	0.9767	0.9867	0.9400	0.9933	<u>0.8600</u>	0.4067	0.4467	0.4033	0.8467	0.9867	0.8533	<u>0.9905</u>
Trace	<u>0.9905</u>	<u>0.9905</u>	<u>0.9905</u>	<u>0.9905</u>	<u>0.9905</u>	<u>0.9905</u>	<u>0.9905</u>	<u>0.9905</u>							

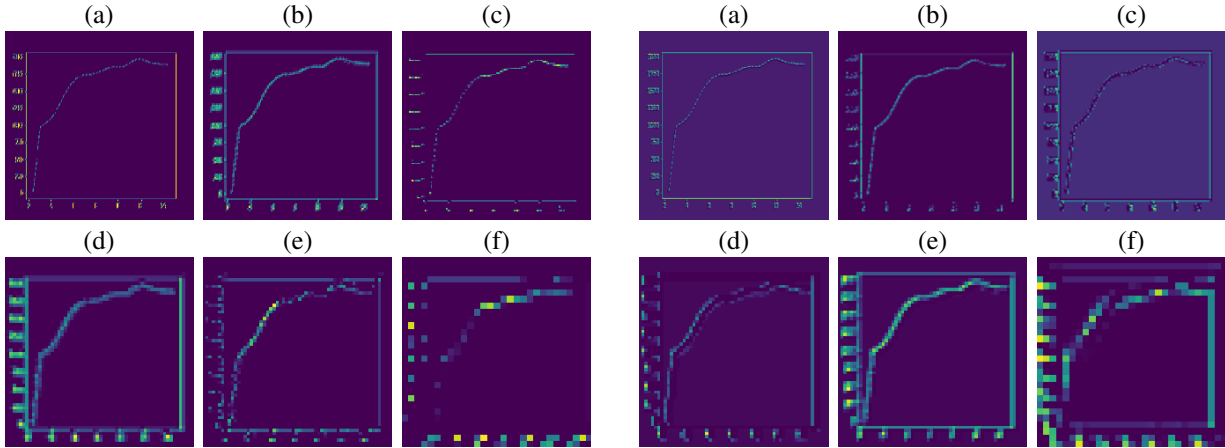


Figure 2: Feature maps from different convolutional layers taken from two models trained on the OPTOX dataset. The set of images on the left side was obtained using input that was normalized, while the right side corresponds to non normalized images. For both set of plots a) was taken from the first convolution layer, b) and c) from the second, d) and e) from the third, and f) from the fourth.

out normalization, there were multiple runs that converged to sub-optimal solutions during training, particularly on the UCR problems. Furthermore, even when the models converged to good solutions, they took much longer to converge than the ones with normalization, as much as $4\times$ longer on the OPTOX dataset.

A possible explanation for this difference is that, without normalization, the filters have to learn the features from low pixel values (curves and axes) that are surrounded by high pixel values (white space), a much more difficult task than the opposite, that is to learn features from the pixels that already enter the network with the highest values. Indeed, when analysing feature maps from models trained with non normalized image data, we observed that sometimes the time series are not even detected in the first convolutional layer. On later layers there are in fact feature maps showing that the filters identified key information such as the time series and axes. However, there are a large number of feature maps where no prominent features are identified, something that

does not happen when the images are normalized.

Figure 2 presents two sets of feature maps. On the left, feature maps obtained from a model trained with normalized data; on the right, feature maps from a model trained on the same dataset (and same training/test partition) without normalization. Comparing both sets, we can see that, with normalization, the filters begin to detect different important areas of the image, starting on the first convolutional layer, whereas without normalization there are almost no activations on the feature maps of the first and second convolutional layers.

6 Conclusions and Future Work

We have proposed a new approach for time series classification where the time series are represented as plot images and given to a shallow CNN. Our methodology is very simple and can be applied to a broad variety of problems, including ones where different time series have different lengths. We tested our methodology on two real-world non public datasets, where it outperformed all other methods, and on the UCR archive,

where it was able to beat the current state-of-the-art methods in a small set of problems. We have also shown that, thanks to the image pre-processing we apply, the models are able to converge faster and detect important image features earlier during training. We conclude that, if a simple naive design like ours can obtain such good results, then there is much to explore when using deep learning methods that rely on image data.

As future research, we will test our methodology using known network architectures such as ResNet, VGG or Inception, and alternative image representations of the data. Finally, we will use the same approach to solve other classification problems that may not involve time series, but rather signal data, such as remote sensing applications.

Acknowledgements

This work was partially supported by FCT through funding of Research Units LASIGE (UIDB/ 00408/2020 and UIDP/ 00408/2020) and MARE (UIDB/ 04292/2020); AICE (DSAIPA/DS/ 0113/2019), Projects BINDER (PTDC/CCI-INF/ 29168/2017), GADgET (DSAIPA/DS/ 0022/2018), INTERPHENO (PTDC/ASP-PLA/ 28726/2017), OPTOX (PTDC/CTA-AMB/ 30056/2017), PREDICT (PTDC/CCI-CIF/ 29877/2017); PhD Grant(SFRH/BD/143972/2019); Research Contracts CEECIND/00511/2017 and CEECIND/02513/2017. The authors also acknowledge Prof. Alberto Rainoldi and Dr. Marco Ivaldi for the useful discussion on the physiological dataset and the Centre of Preventive Medicine and Sport - SUISM - University Structure of Hygiene and Sport Sciences, Centre of Excellence of the University of Torino for allowing the use of the dataset.

References

- [Azzali *et al.*, 2020] Irene Azzali, L. Vanneschi, Ilya Bakurov, Sara Silva, M. Ivaldi, and M. Giacobini. Towards the use of vector based gp to predict physiological time series. *Appl. Soft Comput.*, 89:106097, 2020.
- [Breiman, 2001] Leo Breiman. Random forests. *Machine Learning*, 45:5–32, 2001.
- [Chen and Guestrin, 2016] T. Chen and Carlos Guestrin. Xgboost: A scalable tree boosting system. *Proceedings of the 22nd ACM SIGKDD International Conference on Knowledge Discovery and Data Mining*, 2016.
- [Dau *et al.*, 2018] Hoang Anh Dau, Eamonn Keogh, Kaveh Kamgar, Chin-Chia Michael Yeh, Yan Zhu, Shaghayegh Gharghabi, Chotirat Ann Ratanamahatana, Yanping, Bing Hu, Nurjahan Begum, Anthony Bagnall, Abdullah Mueen, Gustavo Batista, and Hexagon-ML. The ucr time series classification archive, October 2018. https://www.cs.ucr.edu/~eamonn/time_series_data_2018/.
- [Dempster *et al.*, 2020] Angus Dempster, Franccois Petitjean, and Geoffrey I. Webb. Rocket: exceptionally fast and accurate time series classification using random convolutional kernels. *Data Mining and Knowledge Discovery*, 34:1454–1495, 2020.
- [Dovhalets *et al.*, 2018] Dmytro Dovhalets, Boris Kovalerchuk, Szilárd Vajda, and Răzvan Andonie. Deep learning of 2-d images representing n-d data in general line coordinates. In *International Symposium on Affective Science and Engineering*, volume ISASE2018, pages 1–6. Japan Society of Kansei Engineering, 2018.
- [Fawaz *et al.*, 2020] Hassan Ismail Fawaz, B. Lucas, G. Forestier, Charlotte Pelletier, D. Schmidt, Jonathan Weber, Geoffrey I. Webb, L. Idoumghar, Pierre-Alain Muller, and Franccois Petitjean. Inceptiontime: Finding alexnet for time series classification. *ArXiv*, abs/1909.04939, 2020.
- [Hunter, 2007] J. D. Hunter. Matplotlib: A 2d graphics environment. *Computing in Science & Engineering*, 9(3):90–95, 2007.
- [Karimi-Bidhendi *et al.*, 2018] S. Karimi-Bidhendi, F. Munshi, and A. Munshi. Scalable classification of univariate and multivariate time series. In *2018 IEEE International Conference on Big Data*, pages 1598–1605, 2018.
- [Keim, 2000] D. A. Keim. Designing pixel-oriented visualization techniques: theory and applications. *IEEE Transactions on Visualization and Computer Graphics*, 6(1):59–78, 2000.
- [Kovalerchuk, 2018] Boris Kovalerchuk. *Visual Knowledge Discovery and Machine Learning*. Springer International Publishing, 2018.
- [Large *et al.*, 2018] J. Large, Anthony J. Bagnall, S. Malinowski, and R. Tavenard. From bop to boss and beyond: Time series classification with dictionary based classifiers. *ArXiv*, abs/1809.06751, 2018.
- [Lines *et al.*, 2016] J. Lines, Sarah Taylor, and Anthony J. Bagnall. Hive-cote: The hierarchical vote collective of transformation-based ensembles for time series classification. *2016 IEEE ICDM*, pages 1041–1046, 2016.
- [Lucas *et al.*, 2019] B. Lucas, Ahmed Shifaz, Charlotte Pelletier, Lachlan O’Neill, N. A. Zaidi, B. Goethals, François

- Petitjean, and Geoffrey I. Webb. Proximity forest: an effective and scalable distance-based classifier for time series. *Data Mining and Knowledge Discovery*, 33:607–635, 2019.
- [Lyu and Haque, 2018] Boyu Lyu and Anamul Haque. Deep learning based tumor type classification using gene expression data. *bioRxiv*, 2018.
- [Schäfer and Leser, 2017] Patrick Schäfer and U. Leser. Fast and accurate time series classification with weasel. *Proceedings of the 2017 ACM on Conference on Information and Knowledge Management*, 2017.
- [Schäfer, 2014] Patrick Schäfer. The boss is concerned with time series classification in the presence of noise. *Data Mining and Knowledge Discovery*, 29:1505–1530, 2014.
- [Sharma *et al.*, 2019] Alok Sharma, Edwin Vans, Daichi Shigemizu, Keith A. Boroevich, and Tatsuhiko Tsunoda. DeepInsight: A methodology to transform a non-image data to an image for convolution neural network architecture. *Scientific Reports*, 9(1), August 2019.
- [Shifaz *et al.*, 2020] Ahmed Shifaz, Charlotte Pelletier, F. Petitjean, and Geoffrey I. Webb. Ts-chief: a scalable and accurate forest algorithm for time series classification. *Data Mining and Knowledge Discovery*, 34:742–775, 2020.
- [Silva *et al.*, 2020] M. Silva, Eduardo Feijão, Ricardo da Cruz de Carvalho, Irina A. Duarte, A. Matos, M. T. Cabrita, A. Barreiro, M. Lemos, S. Novais, João H Marques, I. Caçador, P. Reis-Santos, V. Fonseca, and B. Duarte. Comfortably numb: Ecotoxicity of the non-steroidal anti-inflammatory drug ibuprofen on *phaeodactylum tricoratum*. *Marine environmental research*, 161:105109, 2020.
- [van der Maaten and Hinton, 2008] Laurens van der Maaten and Geoffrey Hinton. Visualizing data using t-sne. *Journal of Machine Learning Research*, 9(86):2579–2605, 2008.

Appendix

A OPTOX p -values

Table 7: Kruskal-Wallis p -values comparing all methods of the contaminant prediction task of the OPTOX dataset. Above the diagonal, we have the results for the test set, and below for the training set. Significant differences ($p < 0.01$) are represented in **green** or **red** when the method on the left is significantly better or worse, respectively.

	RF	XG	ROCKET	ANN	1D CNN	CNN Log	CNN	
RF	—	$1.23e^{-10}$	$2.58e^{-11}$	$2.80e^{-11}$	$1.89e^{-08}$	$2.68e^{-11}$	$2.63e^{-11}$	Test
XG	$2.24e^{-11}$	—	$2.60e^{-11}$	$2.82e^{-11}$	$1.01e^{-07}$	$2.70e^{-11}$	$2.65e^{-11}$	
ROCKET	$1.88e^{-11}$	$1.08e^{-05}$	—	$2.59e^{-11}$	$4.04e^{-03}$	$5.79e^{-04}$	$3.64e^{-02}$	
ANN	$2.82e^{-11}$	$2.26e^{-11}$	$1.90e^{-11}$	—	$7.04e^{-04}$	$2.69e^{-11}$	$2.64e^{-11}$	
1D CNN	$2.34e^{-11}$	$8.89e^{-02}$	$8.08e^{-01}$	$2.36e^{-11}$	—	$2.68e^{-06}$	$3.19e^{-04}$	
CNN Log	$1.63e^{-09}$	$2.07e^{-11}$	$1.73e^{-11}$	$2.61e^{-11}$	$6.55e^{-09}$	—	$6.93e^{-03}$	
CNN	$2.54e^{-11}$	$2.03e^{-11}$	$1.70e^{-11}$	$2.56e^{-11}$	$3.09e^{-08}$	$2.55e^{-02}$	—	
				Training				

B FISIO p -values

Table 8: Kruskal-Wallis p -values comparing all methods of the BMI.Siamese prediction task. Above the diagonal, we have the results for the test set, and below for the training set. Significant results ($p < 0.01$) are represented in **green** or **red** when the method on the left is significantly better or worse, respectively.

BMI.Siamese	ANN	1D CNN	CNN	
ANN	—	$8.31e^{-10}$	$4.76e^{-01}$	Test
1D CNN	$1.12e^{-11}$	—	$1.32e^{-09}$	
CNN	$1.04e^{-12}$	$6.33e^{-04}$	—	
		Training		

Table 9: Kruskal-Wallis p -values comparing all methods of the BMI.HR prediction task. Above the diagonal, we have the results for the test set, and below for the training set. Significant results ($p < 0.01$) are represented in **green** or **red** when the method on the left is significantly better or worse, respectively.

BMI.HR	RF	XG	Rocket	ANN	1D CNN	CNN	
RF	—	$9.94e^{-01}$	$2.34e^{-08}$	$7.81e^{-07}$	$2.25e^{-11}$	$6.55e^{-01}$	Test
XG	$1.00e^{+00}$	—	$3.11e^{-08}$	$2.96e^{-06}$	$2.24e^{-11}$	$7.32e^{-01}$	
Rocket	$1.10e^{-12}$	$1.12e^{-12}$	—	$3.52e^{-04}$	$7.29e^{-05}$	$1.48e^{-08}$	
ANN	$5.89e^{-08}$	$1.30e^{-10}$	$1.06e^{-12}$	—	$1.22e^{-10}$	$1.86e^{-08}$	
1D CNN	$8.88e^{-12}$	$7.31e^{-12}$	$5.35e^{-03}$	$8.18e^{-12}$	—	$1.96e^{-11}$	
CNN	$1.10e^{-12}$	$1.12e^{-12}$	$1.00e^{+00}$	$1.06e^{-12}$	$5.35e^{-03}$	—	
			Training				

Table 10: Kruskal-Wallis p -values comparing all methods of the BMI.VEN prediction task. Above the diagonal, we have the results for the test set, and below for the training set. Significant results ($p < 0.01$) are represented in **green** or **red** when the method on the left is significantly better or worse, respectively.

BMI.VEN	RF	XG	Rocket	ANN	1D CNN	CNN	
RF	—	$9.11e^{-01}$	$2.33e^{-07}$	$4.21e^{-03}$	$8.82e^{-11}$	$3.97e^{-01}$	Test
XG	$4.69e^{-01}$	—	$3.99e^{-07}$	$4.83e^{-03}$	$2.31e^{-10}$	$4.06e^{-01}$	
Rocket	$1.13e^{-12}$	$1.12e^{-12}$	—	$6.07e^{-04}$	$3.41e^{-05}$	$8.08e^{-08}$	
ANN	$1.34e^{-02}$	$5.64e^{-05}$	$1.07e^{-12}$	—	$3.52e^{-09}$	$9.34e^{-03}$	
1D CNN	$5.65e^{-11}$	$1.04e^{-10}$	$1.54e^{-01}$	$1.13e^{-09}$	—	$2.73e^{-11}$	
CNN	$1.13e^{-12}$	$1.12e^{-12}$	$1.00e^{+00}$	$1.07e^{-12}$	$1.54e^{-01}$	—	
			Training				

Table 11: Kruskal-Wallis p -values comparing all methods of the BMI.HR+VEN prediction task. Above the diagonal, we have the results for the test set, and below for the training set. Significant results ($p < 0.01$) are represented in **green** or **red** when the method on the left is significantly better or worse, respectively.

BMI.HR+VEN	RF	XG	Rocket	ANN	1D CNN	CNN	
RF	—	$8.11e^{-01}$	$1.77e^{-08}$	$2.21e^{-05}$	$2.57e^{-11}$	$4.28e^{-01}$	Test
XG	$8.94e^{-01}$	—	$3.47e^{-09}$	$2.72e^{-06}$	$2.49e^{-11}$	$3.31e^{-01}$	
Rocket	$1.12e^{-12}$	$4.28e^{-12}$	—	$8.03e^{-04}$	$2.60e^{-11}$	$4.55e^{-10}$	
ANN	$1.25e^{-03}$	$7.09e^{-07}$	$1.08e^{-12}$	—	$2.44e^{-11}$	$7.22e^{-07}$	
1D CNN	$2.66e^{-11}$	$2.67e^{-11}$	$1.06e^{-12}$	$2.57e^{-11}$	—	$1.69e^{-11}$	
CNN	$1.12e^{-12}$	$4.28e^{-12}$	$1.00e^{+00}$	$1.08e^{-12}$	$1.06e^{-12}$	—	
			Training				

Table 12: Kruskal-Wallis p -values comparing all methods of the Age.Siamese prediction task. Above the diagonal, we have the results for the test set, and below for the training set. Significant results ($p < 0.01$) are represented in **green** or **red** when the method on the left is significantly better or worse, respectively.

Age.Siamese	ANN	1D CNN	CNN	
ANN	—	$5.11e^{-01}$	$3.13e^{-01}$	Test
1D CNN	$2.10e^{-11}$	—	$6.33e^{-02}$	
CNN	$1.12e^{-12}$	$5.09e^{-06}$	—	
		Training		

Table 13: Kruskal-Wallis p -values comparing all methods of the Age.HR prediction task. Above the diagonal, we have the results for the test set, and below for the training set. Significant results ($p < 0.01$) are represented in **green** or **red** when the method on the left is significantly better or worse, respectively.

Age.HR	RF	XG	Rocket	ANN	1D CNN	CNN	
RF	—	$6.51e^{-01}$	$8.99e^{-01}$	$3.82e^{-01}$	$1.51e^{-02}$	$6.23e^{-08}$	Test
XG	$1.51e^{-01}$	—	$6.71e^{-01}$	$1.55e^{-01}$	$3.41e^{-02}$	$1.76e^{-08}$	
Rocket	$1.55e^{-11}$	$1.53e^{-11}$	—	$2.54e^{-01}$	$2.75e^{-03}$	$1.55e^{-09}$	
ANN	$1.18e^{-05}$	$2.37e^{-07}$	$1.08e^{-12}$	—	$1.35e^{-03}$	$4.58e^{-07}$	
1D CNN	$4.05e^{-09}$	$3.04e^{-09}$	$5.32e^{-03}$	$8.64e^{-12}$	—	$8.02e^{-11}$	
CNN	$1.55e^{-11}$	$1.53e^{-11}$	$1.00e^{+00}$	$1.08e^{-12}$	$5.32e^{-03}$	—	
			Training				

Table 14: Kruskal-Wallis p -values comparing all methods of the Age.VEN prediction task. Above the diagonal, we have the results for the test set, and below for the training set. Significant results ($p < 0.01$) are represented in **green** or **red** when the method on the left is significantly better or worse, respectively.

Age.VEN	RF	XG	Rocket	ANN	1D CNN	CNN	
RF	—	$3.25e^{-01}$	$6.64e^{-02}$	$6.57e^{-01}$	$4.39e^{-02}$	$7.97e^{-04}$	Test
XG	$2.71e^{-01}$	—	$1.19e^{-03}$	$1.16e^{-01}$	$2.08e^{-04}$	$2.03e^{-04}$	
Rocket	$1.52e^{-11}$	$3.29e^{-07}$	—	$1.20e^{-01}$	$7.00e^{-01}$	$5.56e^{-08}$	
ANN	$2.13e^{-01}$	$3.90e^{-02}$	$1.06e^{-12}$	—	$8.67e^{-02}$	$1.68e^{-05}$	
1D CNN	$1.63e^{-07}$	$4.54e^{-04}$	$5.36e^{-03}$	$5.27e^{-10}$	—	$6.99e^{-09}$	
CNN	$1.52e^{-11}$	$3.29e^{-07}$	$1.00e^{+00}$	$1.06e^{-12}$	$5.36e^{-03}$	—	
			Training				

Table 15: Kruskal-Wallis p -values comparing all methods of the Age.HR+VEN prediction task. Above the diagonal, we have the results for the test set, and below for the training set. Significant results ($p < 0.01$) are represented in **green** or **red** when the method on the left is significantly better or worse, respectively.

Age.HR+VEN	RF	XG	Rocket	ANN	1D CNN	CNN	
RF	—	$7.88e^{-03}$	$6.68e^{-03}$	$7.65e^{-04}$	$6.61e^{-02}$	$3.58e^{-04}$	Test
XG	$1.99e^{-03}$	—	$5.02e^{-01}$	$1.68e^{-01}$	$5.63e^{-01}$	$1.23e^{-01}$	
Rocket	$1.79e^{-10}$	$3.00e^{-04}$	—	$5.73e^{-01}$	$9.10e^{-02}$	$3.58e^{-01}$	
ANN	$8.33e^{-02}$	$2.91e^{-05}$	$1.10e^{-12}$	—	$8.70e^{-03}$	$9.06e^{-01}$	
1D CNN	$2.25e^{-08}$	$1.16e^{-02}$	$7.82e^{-02}$	$7.44e^{-11}$	—	$5.57e^{-03}$	
CNN	$1.79e^{-10}$	$3.00e^{-04}$	$1.00e^{+00}$	$1.10e^{-12}$	$7.82e^{-02}$	—	
			Training				

C UCR p -values

Table 16: Kruskal-Wallis p -values comparing the test results of all methods on the BME prediction task. Significant results ($p < 0.01$) are represented in **green** or **red** when the method on the left is significantly better or worse, respectively.

BME	TS-CHIEF	HIVE-COTE v1.0	ROCKET	Inception Time	STC	ResNet	Proximity Forest	WEASEL	S-BOSS	cBOSS	BOSS	RISE	TSF	Catch22	Test
CNN	$1.26e^{-01}$	$1.35e^{-04}$	$1.20e^{-01}$	$3.81e^{-01}$	$3.02e^{-11}$	$1.02e^{-03}$	$5.50e^{-09}$	$9.16e^{-08}$	$3.06e^{-11}$	$3.05e^{-11}$	$3.08e^{-11}$	$3.07e^{-11}$	$4.74e^{-09}$	$3.07e^{-11}$	
TS-CHIEF		$2.75e^{-06}$	$8.53e^{-01}$	$3.24e^{-01}$	$3.18e^{-11}$	$1.49e^{-02}$	$1.71e^{-01}$	$1.10e^{-08}$	$2.10e^{-11}$	$2.09e^{-11}$	$2.11e^{-11}$	$1.99e^{-11}$	$4.14e^{-10}$	$2.35e^{-11}$	
HIVE-COTE v1.0			$1.34e^{-06}$		$8.76e^{-10}$	$5.93e^{-09}$	$1.28e^{-08}$	$6.09e^{-04}$	$8.83e^{-11}$	$6.46e^{-11}$	$7.61e^{-11}$	$5.55e^{-11}$	$1.12e^{-03}$	$1.72e^{-10}$	
ROCKET				$3.96e^{-01}$	$2.33e^{-11}$	$7.95e^{-03}$	$1.10e^{-01}$	$6.19e^{-09}$	$2.24e^{-11}$	$2.23e^{-11}$	$2.25e^{-11}$	$2.24e^{-11}$	$7.95e^{-11}$	$2.24e^{-11}$	
InceptionTime					$3.19e^{-11}$	$9.81e^{-04}$	$1.66e^{-02}$	$2.06e^{-08}$	$3.06e^{-11}$	$3.05e^{-11}$	$3.08e^{-11}$	$3.07e^{-11}$	$2.45e^{-10}$	$3.07e^{-11}$	
STC						$3.95e^{-12}$	$8.82e^{-12}$	$1.03e^{-02}$	$4.95e^{-06}$	$5.21e^{-09}$	$2.19e^{-06}$	$7.59e^{-11}$	$1.84e^{-04}$	$7.67e^{-03}$	
ResNet							$1.85e^{-01}$	$1.54e^{-10}$	$3.79e^{-12}$	$3.78e^{-12}$	$3.82e^{-12}$	$3.80e^{-12}$	$1.48e^{-11}$	$3.81e^{-12}$	
ProximityForest								$3.76e^{-10}$	$8.97e^{-12}$	$8.93e^{-12}$	$9.03e^{-12}$	$8.97e^{-12}$	$8.78e^{-12}$	$8.99e^{-12}$	
WEASEL									$4.93e^{-07}$	$5.84e^{-09}$	$2.38e^{-07}$	$9.13e^{-10}$	$4.13e^{-01}$	$4.82e^{-05}$	
S-BOSS										$1.58e^{-04}$	$9.56e^{-01}$	$3.90e^{-06}$	$1.59e^{-09}$	$4.65e^{-03}$	
cBOSS											$1.76e^{-05}$	$8.39e^{-01}$	$1.99e^{-10}$	$1.05e^{-07}$	
BOSS												$1.01e^{-07}$	$7.00e^{-10}$	$2.78e^{-03}$	
RISE													$5.83e^{-11}$	$8.62e^{-10}$	
TSF														$1.00e^{-07}$	

Table 17: Kruskal-Wallis p -values comparing the test results of all methods on the Coffee prediction task. Significant results ($p < 0.01$) are represented in **green** or **red** when the method on the left is significantly better or worse, respectively.

Coffee	TS-CHIEF	HIVE-COTE v1.0	ROCKET	Inception Time	STC	ResNet	Proximity Forest	WEASEL	S-BOSS	cBOSS	BOSS	RISE	TSF	Catch22	Test
CNN	$2.53e^{-03}$	$2.05e^{-02}$	$1.00e^{+00}$	$3.17e^{-01}$	$5.20e^{-03}$	$7.79e^{-02}$	$1.04e^{-02}$	$2.56e^{-03}$	$2.25e^{-05}$	$2.53e^{-03}$	$5.90e^{-04}$	$5.90e^{-04}$	$1.25e^{-03}$	$2.32e^{-05}$	
TS-CHIEF		$3.96e^{-01}$	$2.53e^{-03}$	$1.18e^{-02}$	$8.30e^{-01}$	$9.69e^{-02}$	$6.01e^{-01}$	$9.36e^{-01}$	$8.17e^{-02}$	$1.00e^{+00}$	$4.76e^{-01}$	$4.76e^{-01}$	$3.27e^{-01}$	$7.07e^{-02}$	
HIVE-COTE v1.0			$2.05e^{-02}$	$8.49e^{-02}$	$5.29e^{-01}$	$4.28e^{-01}$	$7.49e^{-01}$	$3.68e^{-01}$	$1.50e^{-02}$	$3.96e^{-01}$	$1.40e^{-01}$	$1.37e^{-01}$	$1.38e^{-01}$	$1.34e^{-02}$	
ROCKET				$3.17e^{-01}$	$5.20e^{-03}$	$7.79e^{-02}$	$1.04e^{-02}$	$2.56e^{-03}$	$2.25e^{-05}$	$2.53e^{-03}$	$5.90e^{-04}$	$5.90e^{-04}$	$1.25e^{-03}$	$2.32e^{-05}$	
InceptionTime					$2.29e^{-02}$	$3.04e^{-01}$	$4.45e^{-02}$	$1.16e^{-02}$	$1.11e^{-04}$	$1.18e^{-02}$	$2.69e^{-03}$	$2.69e^{-03}$	$4.33e^{-03}$	$1.10e^{-04}$	
STC						$1.58e^{-01}$	$7.56e^{-01}$	$7.83e^{-01}$	$6.37e^{-02}$	$8.30e^{-01}$	$3.84e^{-01}$	$3.79e^{-01}$	$3.08e^{-01}$	$5.70e^{-02}$	
ResNet							$2.65e^{-01}$	$9.07e^{-02}$	$1.45e^{-03}$	$9.69e^{-02}$	$2.51e^{-02}$	$2.51e^{-02}$	$2.70e^{-02}$	$1.34e^{-03}$	
ProximityForest								$5.59e^{-01}$	$3.18e^{-02}$	$6.01e^{-01}$	$2.40e^{-01}$	$2.36e^{-01}$	$2.13e^{-01}$	$2.80e^{-02}$	
WEASEL									$1.08e^{-01}$	$9.36e^{-01}$	$5.39e^{-01}$	$5.32e^{-01}$	$4.21e^{-01}$	$9.42e^{-02}$	
S-BOSS										$8.17e^{-02}$	$3.35e^{-01}$	$3.44e^{-01}$	$6.26e^{-01}$	$9.03e^{-01}$	
cBOSS											$4.76e^{-01}$	$4.76e^{-01}$	$3.27e^{-01}$	$7.07e^{-02}$	
BOSS												$9.85e^{-01}$	$8.15e^{-01}$	$2.94e^{-01}$	
RISE													$8.15e^{-01}$	$3.06e^{-01}$	
TSF														$5.18e^{-01}$	

Table 18: Kruskal-Wallis p -values comparing the test results of all methods on the Earthquakes prediction task. Significant results ($p < 0.01$) are represented in **green** or **red** when the method on the left is significantly better or worse, respectively.

Earthquakes	TS-CHIEF	HIVE-COTE v1.0	ROCKET	Inception Time	STC	ResNet	Proximity Forest	WEASEL	S-BOSS	cBOSS	BOSS	RISE	TSF	Catch22	Test
CNN	$1.47e^{-03}$	$1.54e^{-03}$	$1.59e^{-03}$	$1.38e^{-05}$	$4.22e^{-04}$	$2.46e^{-08}$	$7.31e^{-03}$	$1.54e^{-03}$	$1.54e^{-03}$	$1.54e^{-03}$	$1.49e^{-03}$	$1.47e^{-03}$	$1.72e^{-03}$	$3.81e^{-04}$	
TS-CHIEF		$7.79e^{-02}$	$3.17e^{-01}$	$5.40e^{-06}$	$3.96e^{-06}$	$2.53e^{-10}$	$3.27e^{-02}$	$7.79e^{-02}$	$7.79e^{-02}$	$7.79e^{-02}$	$2.56e^{-03}$	$1.00e^{+00}$	$1.50e^{-07}$	$5.73e^{-07}$	
HIVE-COTE v1.0			$4.54e^{-02}$	$3.81e^{-05}$	$2.42e^{-04}$	$1.09e^{-09}$	$1.92e^{-02}$	$1.00e^{+00}$	$1.00e^{+00}$	$1.00e^{+00}$	$9.07e^{-02}$	$7.79e^{-02}$	$2.69e^{-07}$	$1.06e^{-05}$	
ROCKET				$5.54e^{-06}$	$3.28e^{-10}$	$5.32e^{-02}$	$5.32e^{-02}$	$4.54e^{-02}$	$4.54e^{-02}$	$4.54e^{-02}$	$1.76e^{-03}$	$3.17e^{-01}$	$1.71e^{-06}$	$5.64e^{-07}$	
InceptionTime					$3.43e^{-02}$	$7.25e^{-03}$	$1.84e^{-04}$	$3.81e^{-05}$	$3.81e^{-05}$	$3.81e^{-05}$	$6.29e^{-04}$	$5.40e^{-06}$	$4.38e^{-06}$	$2.92e^{-01}$	
STC						$7.84e^{-07}$	$4.54e^{-04}$	$2.42e^{-04}$	$2.42e^{-04}$	$2.42e^{-04}$	$2.55e^{-02}$	$3.96e^{-06}$	$1.96e^{-07}$	$1.13e^{-01}$	
ResNet							$5.97e^{-08}$	$1.09e^{-09}$	$1.09e^{-09}$	$1.09e^{-09}$	$8.98e^{-09}$	$2.53e^{-10}$	$1.55e^{-09}$	$1.82e^{-05}$	
ProximityForest								$1.92e^{-02}$	$1.92e^{-02}$	$1.92e^{-02}$	$6.54e^{-03}$	$3.27e^{-02}$	$6.34e^{-01}$	$1.73e^{-04}$	
WEASEL									$1.00e^{+00}$	$1.00e^{+00}$	$9.07e^{-02}$	$7.79e^{-02}$	$2.69e^{-07}$	$1.06e^{-05}$	
S-BOSS										$1.00e^{+00}$	$9.07e^{-02}$	$7.79e^{-02}$	$2.69e^{-07}$	$1.06e^{-05}$	
cBOSS											$9.07e^{-02}$	$7.79e^{-02}$	$2.69e^{-07}$	$1.06e^{-05}$	
BOSS												$2.56e^{-03}$	$3.59e^{-07}$	$6.30e^{-04}$	
RISE													$1.50e^{-07}$	$5.73e^{-07}$	
TSF														$1.26e^{-07}$	

D UCR problems

Table 22: Ranking by dataset from the set of algorithms present in UCR and our CNN methodology on the selected 98 UCR problems.

	1 st	2 nd
ACSF1	ResNet (0.9300)	Over 2 methods (0.9200)
Adiac	InceptionTime (0.8517)	ResNet (0.8491)
ArrowHead	TS-CHIEF & ProximityForest (0.9486)	
Beef	STC (1.0000)	WEASEL & RISE (0.9333)
BeetleFly	Over 2 methods (1.0000)	
BirdChicken	Over 2 methods (1.0000)	
BME	Over 2 methods (1.0000)	
Car	InceptionTime (0.9667)	Over 2 methods (0.9500)
CBF	Over 2 methods (1.0000)	
Chinatown	InceptionTime (0.9883)	ResNet (0.9855)
ChlorineConcentration	InceptionTime (0.8930)	ResNet (0.8703)
CinCECGTorso	HIVE-COTE v1.0 (1.0000)	WEASEL (0.9993)
Coffee	Over 2 methods (1.0000)	
Computers	InceptionTime (0.9040)	ResNet (0.8920)
Crop	InceptionTime (0.7968)	HIVE-COTE v1.0 (0.7730)
DiatomSizeReduction	InceptionTime (1.0000)	ROCKET & BOSS (0.9935)
DistalPhalanxOutlineAgeGroup	S-BOSS (0.9065)	Over 2 methods (0.8993)
DistalPhalanxOutlineCorrect	ROCKET & ProximityForest (0.8696)	
DistalPhalanxTW	Over 2 methods (0.7410)	
Earthquakes	CNN (0.7770)	ProximityForest (0.7698)
ECG200	ResNet (0.9500)	ROCKET & InceptionTime (0.9400)
ECG5000	TS-CHIEF (0.9520)	WEASEL (0.9513)
ECGFiveDays	Over 2 methods (1.0000)	
ElectricDevices	ROCKET (0.9046)	InceptionTime (0.9042)
EthanolLevel	ResNet (0.9080)	InceptionTime (0.9040)
FaceAll	InceptionTime & ResNet (0.9941)	
FaceFour	Over 2 methods (1.0000)	
FacesUCR	InceptionTime (0.9859)	TS-CHIEF (0.9839)
FiftyWords	TS-CHIEF & InceptionTime (0.8659)	
Fish	Over 2 methods (1.0000)	
FordA	WEASEL (0.9765)	InceptionTime (0.9689)
FreezerRegularTrain	HIVE-COTE v1.0 & STC (1.0000)	
FreezerSmallTrain	HIVE-COTE v1.0 & STC (1.0000)	
GunPoint	Over 2 methods (1.0000)	
GunPointAgeSpan	Over 2 methods (1.0000)	
GunPointMaleVersusFemale	Over 2 methods (1.0000)	
GunPointOldVersusYoung	Over 2 methods (1.0000)	
Ham	ProximityForest (1.0000)	ROCKET (0.9968)
Haptics	HIVE-COTE v1.0 (0.9486)	ResNet (0.9351)
Herring	Catch22 (0.9054)	S-BOSS (0.7344)
HouseTwenty	Over 2 methods (0.9916)	
InlineSkate	HIVE-COTE v1.0 (1.0000)	Over 2 methods (0.9916)
InsectEPGRegularTrain	Over 2 methods (1.0000)	
InsectEPGSmallTrain	Over 2 methods (1.0000)	
ItalyPowerDemand	TS-CHIEF & InceptionTime (0.9728)	
LargeKitchenAppliances	InceptionTime (0.9733)	ResNet (0.9718)
Lightning2	ResNet (0.9760)	HIVE-COTE v1.0 (0.9520)

Lightning7	Catch22 (0.9253)	ProximityForest (0.9180)
Mallat	TS-CHIEF (0.9979)	WEASEL (0.9851)
Meat	Over 2 methods (1.0000)	
MedicalImages	Over 2 methods (1.0000)	
MiddlePhalanxOutlineAgeGroup	Catch22 (0.9833)	ROCKET (0.8289)
MiddlePhalanxOutlineCorrect	STC (0.8694)	InceptionTime (0.8660)
MiddlePhalanxTW	ROCKET (0.8660)	ProximityForest (0.8625)
MixedShapesRegularTrain	TS-CHIEF (0.9810)	InceptionTime & WEASEL (0.9753)
MixedShapesSmallTrain	ResNet (0.9790)	HIVE-COTE v1.0 (0.9769)
MoteStrain	TS-CHIEF (0.9688)	HIVE-COTE v1.0 (0.9662)
OliveOil	Over 2 methods (1.0000)	
OSULeaf	ROCKET & ProximityForest (1.0000)	
PhalangesOutlinesCorrect	HIVE-COTE v1.0 (0.9623)	ROCKET (0.9587)
Phoneme	HIVE-COTE v1.0 & ResNet (0.9667)	
PigAirwayPressure	STC (0.9952)	HIVE-COTE v1.0 & ResNet (0.9876)
PigArtPressure	S-BOSS (1.0000)	Over 2 methods (0.9952)
PigCVP	TS-CHIEF (0.9856)	S-BOSS (0.9808)
Plane	<u>Over 2 methods</u> (1.0000)	
ProximalPhalanxOutlineAgeGroup	ProximityForest (1.0000)	ROCKET (0.9889)
ProximalPhalanxOutlineCorrect	HIVE-COTE v1.0 & ResNet (1.0000)	
ProximalPhalanxTW	HIVE-COTE v1.0 & Catch22 (1.0000)	
RefrigerationDevices	Catch22 (0.9389)	HIVE-COTE v1.0 (0.8878)
Rock	STC (0.9600)	WEASEL (0.9400)
ScreenType	ROCKET (0.9000)	Catch22 (0.8660)
SemgHandGenderCh2	TS-CHIEF (0.9683)	TSF (0.9650)
SemgHandMovementCh2	ProximityForest (0.9800)	ROCKET (0.9500)
SemgHandSubjectCh2	TSF (0.9533)	TS-CHIEF (0.9511)
ShapeletSim	Over 2 methods (1.0000)	
ShapesAll	ROCKET (1.0000)	InceptionTime (0.9600)
SmallKitchenAppliances	HIVE-COTE v1.0 (0.9689)	ROCKET (0.9417)
SmoothSubspace	<u>Over 2 methods</u> (1.0000)	
SonyAIBORobotSurface1	ProximityForest & Catch22 (1.0000)	
SonyAIBORobotSurface2	ROCKET (0.9817)	InceptionTime (0.9748)
StarLightCurves	HIVE-COTE v1.0 & ResNet (1.0000)	
Strawberry	WEASEL (0.9919)	Over 2 methods (0.9892)
SwedishLeaf	ROCKET & ProximityForest (0.9919)	
Symbols	TS-CHIEF (0.9879)	InceptionTime (0.9859)
SyntheticControl	Over 2 methods (1.0000)	
ToeSegmentation1	ROCKET & ProximityForest (1.0000)	
ToeSegmentation2	TS-CHIEF & InceptionTime (0.9923)	
Trace	<u>Over 2 methods</u> (1.0000)	
TwoLeadECG	Over 2 methods (1.0000)	
TwoPatterns	Over 2 methods (1.0000)	
UMD	Over 2 methods (1.0000)	
UWaveGestureLibraryAll	Over 2 methods (1.0000)	
Wafer	Over 2 methods (1.0000)	
Wine	Over 2 methods (1.0000)	
WordSynonyms	ROCKET & ProximityForest (1.0000)	
Worms	HIVE-COTE v1.0 & ResNet (1.0000)	
WormsTwoClass	HIVE-COTE v1.0 & ResNet (1.0000)	
Yoga	cBOSS (0.9373)	InceptionTime (0.9337)